GEOPHYSICAL RESEARCH LETTERS, VOL. 27, NO. 1, PAGES 45-48, JANUARY 1, 2000

Evidence of electron impact ionization in the magnetic pileup boundary of Mars

D. Crider[1,7], P. Cloutier[1], C. Law[1], P. Walker[1], Y. Chen[1], M. Acuña[2], J. Connerney[2], D. Mitchell[3], R. Lin[3], K. Anderson[3], C. Carlson[3], J. McFadden[3], H. Rème[4], C. Mazelle[4], C. d'Uston[4], J. Sauvaud[4], D. Vignes[4], D. Brain[5], and N. Ness[6]

Abstract. A sharp decline in electron fluxes is observed in the Mars Global Surveyor Electron Reflectometer data in conjunction with the magnetic pileup boundary. We examine the characteristics of the evolution of the electron distribution function for one orbit. We determine that the spectra can best be explained by electron impact ionization of oxygen and hydrogen. To reproduce the observed spectral evolution, we construct a model of the effects of electron impact ionization on the electron distribution function as a flow element encounters the neutral atmosphere. Using the observed post-shock electron distribution function, we are able to reproduce the observed flux attenuation. We conclude that electron impact ionization is the physical mechanism responsible for the spectral feature.

1. Introduction

The Mars Global Surveyor (MGS) spacecraft has enabled outstanding new insight into the solar wind interaction with Mars. Mars does not have a significant intrinsic magnetic field [Acuña *et al.*, 1998]. Although Mars has crustal magnetic fields, its ionosphere acts as the primary obstacle to the solar wind [Acuña *et al.*, 1998; Cloutier *et al.*, 1999]. Away from the crustal fields, we can compare the solar wind interaction with Mars to that with other non-magnetic objects, like Venus or comets.

In this paper, we focus one feature in the solar wind interaction with Mars--the magnetic pileup boundary (MPB). The MPB is a region in the post-shock solar wind flow around an obstacle that was originally identified at comets in the Giotto flyby of comet Halley [Neubauer *et al.*, 1986; Mazelle *et al.*, 1989]. It is analogous to the plasma mantle identified by Pioneer Venus *in situ* measurements at Venus [Spenner *et al.*, 1980]. As we show in this letter, MGS provides a unique perspective on this boundary at Mars. The electron fluxes measured by MGS evolve in a systematic manner as the spacecraft crosses the boundary. We investigate this interesting signature in the martian MPB electrons from MGS data. We propose the physics involved in the production of the signature and construct a model to reproduce the observations.

[1]Space Physics & Astronomy Dept., Rice University, Houston, TX
[2]NASA Goddard Space Flight Center, Greenbelt, MD
[3]Space Science Lab., University of California, Berkeley, CA
[4]Centre d'Etude Spatiale Rayonnement, Toulouse, France
[5]Lab. for Atmos. & Space Physics, Univ. Colorado, Boulder, CO
[6]Bartol Research Institute, University of Delaware, Newark, DE
[7]Now a NRC Research Associate at (2)

Paper numbr 1999GL003625.
0094-8276/00/1999GL03625$05.00

2. Observed evolution of the electron distribution function

The magnetic pileup boundary is the region in the post-shock solar wind flow characterized by an increase in magnetic field strength in conjunction with a decrease in electron fluxes with decreasing altitude. In Figure 1 are the MGS magnetometer and electron reflectometer (MAG/ER) time series data for the outbound pass of P231. The orbital geometry is a near-polar orbit with periapsis at 175 km close to the north pole. For this outbound pass, MGS rises as it travels to lower latitudes at 10 a.m. local time. The top panel shows the electron distribution function for 5 energy bins of the ER. The middle panel is the color spectrogram. The lower panel provides the simultaneous magnetic field magnitude measurements from MAG.

In Figure 1, the MPB is the region boxed off, corresponding to the rise in magnetic field. Examining the ER data, we find interesting behavior in the electrons at the MPB. At higher energies, the MPB is characterized by a slow, steady decline in the electrons after the bow shock. Referring to the 314 eV bin on Figure 1, the slow loss of electron flux from 100.707 to 100.711 may be seen on the time axis. The total loss ranges from a factor of 2 at higher energy to as much as 2 orders of magnitude at mid-energy. The most dramatic attenuation is seen here in the 79 eV bin, where the flux quickly drops from the time of 100.707 to 100.708. Continuing up to the lowest energy bins, there is still

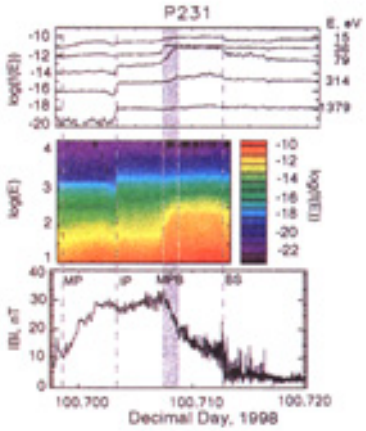

Figure 1. Electron distribution function and magnetic field time series data for P231 outbound. 5 ER energies are given to the right the traces for the top panel. The locations of the ionospheric main peak (MP), ionopause (IP), and bow shock (BS) are given for reference. The magnetic pileup boundary is indicated by the shaded region (MPB).

attenuation in conjunction with the MPB. Below 20 eV, however, the drop is slighter and slower. This signature is typical of the electrons in the MPB for most MGS orbits. Also of note is that the electron flux attenuation occurs within a small spatial extent. The electrons maintain a steady level throughout the sheath from the bow shock until the MPB is reached. Again after the MPB, there is very little variation in the distribution between the bottom of the MPB and the ionopause.

Another way to display the behavior of the electrons in the MPB is to plot their distribution as a function of energy at different times. In Figure 2, we plot one electron spectrum measured by the ER for 6 spacecraft altitudes between 800 and 1050 km, spanning the entire MPB for this orbit. Note that the ER data has an uncertainty in energy of a few eV, based on the amount of spacecraft charging which alters the zero potential of the spacecraft. The counts used within a bin have an uncertainty of ~5%. At the highest altitude, the spectrum is that of the post-shock electrons. The lowest altitude line is the post-MPB spectrum. However, it is the order in which the attenuation proceeds in energy through the MPB that is the interesting feature of this plot. In Figure 2, the distribution function first declines at the highest energy. The 1000 km spectrum first peels off from the post-shock distribution near 200 eV. By 950 km altitude, the spectrum has separated at 79 eV. At this altitude, there is still little attenuation at lower energy. Then, there is a large, sudden drop in the energy bins between 50-150 eV. In P231, it occurs between 850 and 950 km. This signature in the evolution of the electron spectra indicates that some process is removing electrons in the 40-150 eV energy range in the MPB.

That energy range corresponds to where the cross sections for electron impact ionization (EII) of neutral hydrogen and oxygen are high [Shah *et al.*, 1987; Thompson *et al.*, 1995]. In fact, the signature in the electrons is quite reminiscent of EII. Incident electrons impact a particle and kick off a secondary electron. In the process, the incident electron loses kinetic energy equal to the sum of the ionization potential of the atom and the kinetic energy of the ejected electron. The resulting distribution function reflects this by shifting electrons downward in the energy bins. High energy electrons slowly cascade down to lower energy bins as subsequent reactions affect the electrons. The reaction rate for high energy electrons is not very high, but each electron has the energy to react many times before falling below the threshold energy for reaction. That makes EII at high energy a slow, but sustainable process. On the other hand, where the cross section is the highest, there are many reactions and many electrons lost from the bin countered only by slow repopulation by cascading

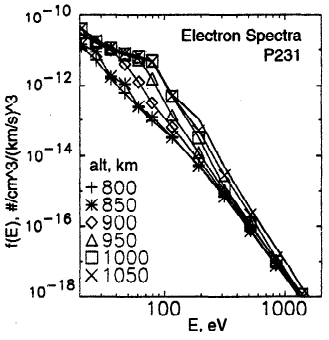

Figure 2. The electron spectra are plotted for several different altitudes within the MPB. The distribution collapses from the topmost trace at 1050 km to the lowest trace at 800 km.

electrons. At the lowest energy, close to the ionization potential, the loss rate of electrons moving out of the energy bins comes close to balancing the rate of repopulation of the low energy bins by cascading and secondary electrons. This explains the limited change in distribution in these bins. Based on EII cross sections, we expect that EII would affect electron distribution functions exactly as seen in the ER data.

Although EII is not a new idea, this work with this data set offers a unique insight on the effects of EII on the electron distribution function. Most previous works at Mars, Venus, and comets assume an initial distribution function of electrons that is usually a Maxwellian or combination of Maxwellians [*e.g.* Haider, 1997; Gan *et al.*, 1990]. Looking at the post-shock spectrum at the top of Figure 2, it is obvious that the electron distribution is not Maxwellian. We use the measured distribution of electrons in our calculations. Also, our goal is much different than other works. Here we strive to reproduce the observed distribution function. Haider and other ionospheric modelers are modeling ion density profiles resulting from many processes including EII. Gan *et al.* try to derive a temperature from heat flow calculations including EII.

3. Model of the interaction

We construct a model to reproduce the electron spectra observed by the MGS ER based on EII of a model planetary exosphere. We start with an average post-shock spectrum measured by the ER for an individual orbit. Although the ER gives us the distribution function at 18 energies ranging from 10 eV to 20 keV, we employ a piecewise exponential function to subdivide the distribution into 5 eV energy bins from 15 eV to 10 keV. Then, we follow the change in the distribution of electrons in a flow element due to EII reactions as the flow encounters the neutral atmosphere.

The evolution of the distribution function is calculated as follows. We compute the reaction rates for all EII reactions with the constituents of the neutral atmosphere (H, O, and CO_2) for each energy bin by integrating the product of the distribution function, the cross section for reaction and the relative velocity of reactants over the relevant velocity space. Then, we redistribute electrons by tabulating the change in number of electrons in each energy bin with each time step. We add new electrons that cascade down from a higher energy bin due to EII reactions and secondary electrons produced with the correct energy. Also, we must subtract the number of electrons in the energy bin that react and, thus, lose enough energy to leave the bin. Knowing the new number of electrons by bin for the next time step, we recover the evolved distribution function. Byproducts of the calculation include ion production rate by species, total energy lost by the electrons, as well as the electron distribution function along a streamline.

The model calculations rely on several input parameters. First of all, we use a post-shock flow velocity given by Spreiter & Stahara [1992; Spreiter *et al.*, 1970]. We include an additional shear layer to reduce the flow speed from the Spreiter Stahara value to 5 km/s in a layer 50-100 km thick at the lower altitude boundary. We incorporate this shear layer to account for the fact that Mars is not an ideal obstacle and that the velocity must not exceed the escape speed at the ionopause. There is observational evidence for the existence of such a layer in the rotation of magnetic field lines in conjunction with the appearance of ionospheric plasma [Cloutier *et al.*, 1999]. The effect was first detected by Law & Cloutier [1995] at Venus. Next, we take the EII

reaction cross sections from experimental data. Cross sections and fractional cross sections for daughter ions from $e^- + CO_2$ are from Straub *et al.* [1996]. EII cross sections for O are from Thompson *et al.* [1995] and those for H are from Shah *et al.* [1987]. Differential cross sections for EII, giving the partition of kinetic energy between resulting electrons, are from Kim & Rudd [1994]. Finally, we implement a neutral density model. For this, we use a compilation of the neutral exosphere of Kim *et al.* [1998] and the low altitude model of Shinigawa & Cravens [1989].

One important point is that the electron thermal velocity is much faster than the local flow speed. These electrons, having gyroradii of < 2 km in the typical magnetic field strength of the sheath, travel a long way along a magnetic field line in the time the flow moves the field line only a short distance (see Figure 3). With any net inclination to the draped magnetic field lines, the electrons being sampled by the spacecraft have seen a range of altitudes and neutral densities. When looking at positions in the flow off of the magnetic noon line, one must consider an effective neutral density over the traverse of the magnetic field line. Because the change in neutral density is exponential with altitude, the effects of EII on the spectrum decrease rapidly over a neutral scale height. Therefore, we estimate the cumulative effects of EII along the extent of the field line by following only the lowest altitude of the magnetic field lines as they flow over the planet at magnetic noon. Computing the reaction rates there, we get the attenuation as electrons pass through the high density region. Then, to account for the fact that only half of the electrons measured by the ER have just passed in front of the planet, we correct our modification to the distribution by a factor of .5.

Finally, we assume that EII is the only process affecting the spectrum of the electrons. The density and distribution function are constant upstream and match the measured post-shock distribution from the ER. Any MHD effect that changes the electron pressure, temperature, and density is not included in this model.

4. Simulation results

Before completing the full-scale calculations described above, we verify that this process is capable of giving the observed spectra. We simulate the evolution of the post-shock electron distribution as it sits in a constant neutral density similar to the martian exosphere and ask if the spectrum can ever achieve the observed spectrum at the bottom of the MPB. In Figure 4, we show that the post-MPB spectrum can be obtained by a simulation using neutral hydrogen. The simulation used the solid line as the input

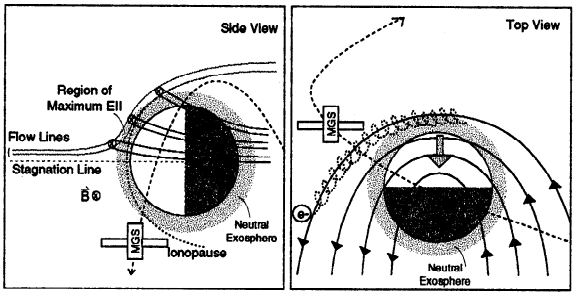

Figure 3. Cartoon of interaction. EII occurs at low altitude, where the neutral density is high. However, draping of magnetic field lines carries the flux tubes to higher altitudes on the flanks of the planet. There, the spacecraft intersects the field line and detects the signature.

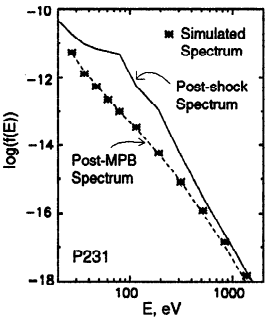

Figure 4. The results of running the model at a constant neutral density indicate that after 4.25e8 s/cm^3 of H, the simulated spectrum has reached the same level of attenuation as the data. The solid line is the average post-shock spectrum for P231 outbound. Feeding this into the model, we obtain the asterisk's (*), which agree well with the dashed line representing the measured spectrum below the MPB.

post-shock spectrum. It is an average post-shock spectrum for P231 taken from the data. The dashed line is the measured spectrum downstream of the MPB. The results of the simulation are the (*) symbols on the plot. After 4.25 x 10^8 s/cm^3 of H (equivalent to a flow element of electrons spending 425 s in a neutral density of 10^6 atoms/cm^3,) the simulated spectrum matches the dashed line very well.

This result implies that the integral of neutral hydrogen density along the flow line over time is on the order of a few times 10^8 s/cm^3. Using a flow speed from the sheath of 50 km/s and a neutral density of 350 km altitude, we find that the flow has to travel 55° around the planet to achieve this integral measure. However, we examine the orbital geometry in a coordinate system aligned with the direction of the upstream IMF and corrected for the aberration of the solar wind. In these magnetic coordinates, the MPB occurs very close to the magnetic equator. Thus, the requirement of 55° of travel contradicts the observations. If the flow speed is reduced to a speed much closer to the ionospheric flow speed, *e.g.* 10 km/s, the travel distance is reduced by a factor of 5 to 11°. That result is far more reasonable given the position of the boundary. Therefore, we conclude that the MPB is formed in the shear layer where flow velocities are reduced.

Finally, using the full scale model run over a number of flow elements, we attempt to reproduce the observed spectra from the MGS data. We implement geometry considerations to trace the spacecraft location to the magnetic noon flow line position. First, we run the model on several flow lines assuming a solar wind speed of 300 km/s. A simple velocity shear model slows the tangential component of the velocity in a layer 50 km thick to 5 km/s at 275 km. Then, to map the coordinates of the spacecraft to where magnetic flux tubes cross the magnetic noon line, we perform the following transformations: 1) We rotate the spacecraft location into magnetic aligned coordinates. 2) We scale the altitude of the points in the MPB such that the thickness at noon is .7 of that at 45°. 3) To account for the spreading of magnetic field lines in latitude, the latitude of the coordinates along noon is twice the spacecraft latitude. Plotting the model results from the positions mapped from the spacecraft position, we obtain the simulated time series electron data in Figure 5. The calculated electron distributions for 11 energy bins are plotted. The fluxes at lowest energy are barely affected by the model, like in the data. In the simulation, the attenuation in flux lasts for longer times

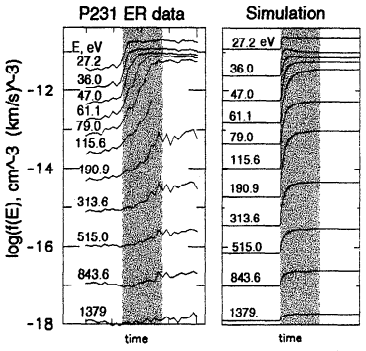

Figure 5. After running the model over several flow lines and mapping the spacecraft trajectory to the simulation space, we reproduce the time series ER data. The left hand panel is the ER data while the right panel is the model results mapped to the spacecraft position. The shaded region in this plot corresponds to the MPB. Energy bins with $27.2 \leq E \leq 1380$ eV are shown.

with increasing electron energy, which also resembles the data. Further, the size of the drop from start to finish agrees very well with the measured values for most energy bins.

Although the two traces are qualitatively the same, a direct comparison would show that the model does not provide a good quantitative fit to the data. Our results for mapping the spacecraft position to the simulation space are extremely model dependent. With as dynamic of an interaction as the solar wind interaction with Mars, we expect these parameters to evolve continuously. Therefore, one cannot compare the parameters found for different orbits to establish a universal solution in the parameter space. Even so, we are able to make reasonable assumptions about the parameters and qualitatively reproduce the data.

5. Conclusions

Our simple model of EII of the martian exosphere reproduces the observed evolution of the electron spectra. Therefore, we are confident that our model represents the underlying physics of the interaction. An important note, however, is that the spacecraft measures the process remotely. The interaction occurs at the lowest altitude of the magnetic field line, which usually is located along magnetic noon. The draping of the field lines around the planet brings flux tubes attached to a low altitude in front of the planet to higher altitudes on the flanks. It is there that MGS happens to cross the flux tubes and detects the signature in the electrons.

Further, we have shown that the model provides an integral measure of the amount of time spent by the electrons in a neutral density. This product can be rewritten as the quotient of neutral density over flow speed integrated over a flow line. The amount of attenuation observed in the electrons defines this quantity. In turn, this quantity constrains the combination of neutral density, flow velocity, and magnetic geometry of the interaction. Existing models [*e.g.* Kim *et al.*, 1998; Spreiter & Stahara, 1992] must conform to the bounds described here.

Finally, the EII process is continually producing new ions out of planetary neutrals above the ionosphere. These ions are vulnerable to pick up by the solar wind. As many of the ions will be subsequently lost, EII is systematically eroding the atmosphere. The relation of EII to the evolution of the martian atmosphere is left for ongoing work.

Acknowledgments. This work was carried out at Rice under NASA grant number NGT 5-34.

References

Acuña, M.H., J.E.P. Connerney, P. Wasilewski, R.P. Lin, K.A. Anderson, C.W. Carlson, J. McFadden, D.W. Curtis, D. Mitchell, H. Rème, C. Mazelle, J.A. Sauvaud, C. d'Uston, A. Cros, J.L. Medale, S.J. Bauer, P. Cloutier, M. Mayhew, D. Winterhalter, and N.F. Ness. Magnetic field and plasma observations at Mars: Initial results of the Mars Global Surveyor Mission, *Science*, **279**, 1676, 1998.

Cloutier, P.A., Y. Chen, D.H. Crider, C.C. Law, P.W. Walker, M.H. Acuña, J.E.P. Connerney, R.P. Lin, K.A. Anderson, D.L. Mitchell, C.W. Carlson, J. McFadden, D.A. Brain, H. Rème, C. Mazelle, J.A. Sauvaud, C. d'Uston, D. Vignes, S.J. Bauer, and N.F. Ness. Venus-like interaction of the solar wind with Mars, *Geophys. Res. Lett.*, **26**, 2685, 1999.

Gan, L., T.E. Cravens, and M. Horanyi. Electrons in the ionopause boundary layer of Venus, *J. Geophys. Res.*, **95**, 19023, 1990.

Haider, S.A. Chemistry of the nightside ionosphere of Mars, *J. Geophys. Res.*, **102**, 407, 1997.

Kim, J., A.F. Nagy, J.L. Fox, and T.E. Cravens. Solar cycle variability of hot oxygen atoms at Mars, *J. Geophys. Res.*, **103**, 29339, 1998.

Kim, Y.-K. and M. E. Rudd. Binary-encounter-dipole model for electron-impact ionization, *Phys. Rev. A*, **50**, 5, 3954, 1994.

Law, C.C. and P.A. Cloutier. Observations of magnetic structure at the dayside ionopause of Venus, *J. Geophys. Res.*, **100**, 23973, 1995.

Mazelle, C., H. Rème, J.A. Sauvaud, C. d'Uston, C.W. Carlson, K.A. Anderson, D.W. Curtis, R.P. Lin, A. Korth, D.A. Mendis, F.M. Neubauer, K.-H. Glassmeier, and J. Raeder. Analysis of suprathermal electron properties at the magnetic pile-up boundary of comet P/Halley, *Geophys. Res. Let.*, **16**, 9, 1035, 1989.

Neubauer, F.M. Giotto magnetic-field results on the boundaries of the pile-up region and the magnetic cavity, *Astron. & Astrophys.*, **187**, 73, 1987.

Shah, M.B., D.S. Elliott, and H.B. Gilbody. Pulsed cross-beam study of the ionisation of atomic hydrogen by electron impact, *J. Phys. B*, **20**, 3501, 1987.

Shinagawa, H. and T.E. Cravens. A one dimensional multispecies magnetohydrodynamic model of the dayside ionosphere of Mars, *J. Geophys. Res.*, **94**, 6506, 1989.

Spenner, K., W.C. Knudsen, K.L. Miller, V. Novak, C.T. Russell, and R.C. Elphic. Observations of the Venus mantle, the boundary layer between solar wind and ionosphere, *J. Geophys. Res.*, **85**, 7655, 1980.

Spreiter, J.R., A.L. Summers, and A.W. Rizzi. Solar wind flow past nonmagnetic planets--Venus and Mars, *Plan. Space Sci.*, **18**, 1281, 1970.

Spreiter, J.R. and S.S. Stahara. Computer modeling of the solar wind interaction with Venus and Mars, *Venus and Mars: Atmospheres, Ionospheres, and Solar Wind Interactions*, J.G. Luhmann, M. Tatrallyay, and R.O. Pepin, eds. Geophysical Monograph **66**, 345, 1992.

Straub, H.C., B.G. Lindsay, K.A. Smith, and R. F. Stebbings. Absolute partial cross sections for electron-impact ionization of CO_2 from threshold to 1000 eV, *J. Chem. Phys.*, **105**, 10, 4015, 1996.

Thompson, W.R., M.B. Shah, and H.B. Gilbody. Single and double ionization of atomic oxygen by electron impact, *J. Phys. B*, **28**, 1321, 1995.

P. Cloutier, C. Law, Y. Chen, and P. Walker, Dept. of Space Physics & Astronomy, Rice Univ., Houston, TX 77005

D. Crider, M. Acuña, and J. Connerney, NASA Goddard Space Flight Center, Greenbelt, MD 20771 (dcrider@lepvax.gsfc.nasa.gov)

D. Mitchell, R. Lin, K. Anderson, C. Carlson and J. McFadden, Space Science Lab., Univ. California, Berkeley, CA 94720

H. Rème, C. Mazelle, C. D'Uston, J. Sauvaud, and D. Vignes, CESR/CNRS, Univ. Paul Sabatier, Toulouse 31029, France

D. Brain, Lab. for Atmospheric & Space Physics, Univ. Colorado, Boulder, CO 80309

N. Ness, Bartol Research Inst., Univ. Delaware, Newark, DE 19716

(Received June 22, 1999; revised September 23, 1999; accepted October 22, 1999.)